

Article

Conversion of Argan Nutshells into Novel Porous Carbons in the Scope of Circular Economy: Adsorption Performance of Emerging Contaminants

Asma Mokhati ^{1,*} , Oumessaâd Benturki ¹, Asma Benturki ¹, Radia Fennouh ¹, Zoubida Kecira ¹, Maria Bernardo ^{2,*} , Inês Matos ², Nuno Lapa ² , Márcia Ventura ², Olívia Salomé G. P. Soares ^{3,4} , Ana M. Botelho Do Rego ^{5,6}  and Isabel Fonseca ²

¹ Laboratory of Physical and Chemical Study of Materials and Applications in the Environment, Faculty of Chemistry (USTHB), El Alia BP 32-16111, Algeria; obenturki2013@gmail.com (O.B.); asmaben82@yahoo.fr (A.B.); radia_fennouh@yahoo.fr (R.F.); z_kecira@yahoo.com (Z.K.)

² LAQV/REQUIMTE, Faculdade de Ciências e Tecnologia, Universidade Nova de Lisboa, 2829-516 Caparica, Portugal; ines.matos@fct.unl.pt (I.M.); ncsn@fct.unl.pt (N.L.); mm.ventura@fct.unl.pt (M.V.); blo@fct.unl.pt (I.F.)

³ Laboratory of Separation and Reaction Engineering—Laboratory of Catalysis and Materials (LSRE-LCM), Faculty of Engineering, University of Porto, Rua Dr. Roberto Frias, 4200-465 Porto, Portugal; salome.soares@fe.up.pt

⁴ ALiCE—Associate Laboratory in Chemical Engineering, Faculty of Engineering, University of Porto, Rua Dr. Roberto Frias, 4200-465 Porto, Portugal

⁵ BSIRG, IBB—Institute for Bioengineering and Biosciences, Departamento de Engenharia Química, Instituto Superior Técnico, Universidade de Lisboa, 1049-001 Lisboa, Portugal; amrego@tecnico.ulisboa.pt

⁶ Associate Laboratory i4HB—Institute for Health and Bioeconomy at Instituto Superior Técnico, Universidade de Lisboa, Av. Rovisco Pais, 1049-001 Lisboa, Portugal

* Correspondence: amokhati@usthb.dz (A.M.); maria.b@fct.unl.pt (M.B.); Tel.: +213-699586861 (A.M.); +351-212948300 (M.B.)



Citation: Mokhati, A.; Benturki, O.; Benturki, A.; Fennouh, R.; Kecira, Z.; Bernardo, M.; Matos, I.; Lapa, N.; Ventura, M.; Soares, O.S.G.P.; et al. Conversion of Argan Nutshells into Novel Porous Carbons in the Scope of Circular Economy: Adsorption Performance of Emerging Contaminants. *Appl. Sci.* **2022**, *12*, 7607. <https://doi.org/10.3390/app12157607>

Academic Editor: María Ángeles Martín-Lara

Received: 7 June 2022

Accepted: 25 July 2022

Published: 28 July 2022

Publisher's Note: MDPI stays neutral with regard to jurisdictional claims in published maps and institutional affiliations.



Copyright: © 2022 by the authors. Licensee MDPI, Basel, Switzerland. This article is an open access article distributed under the terms and conditions of the Creative Commons Attribution (CC BY) license (<https://creativecommons.org/licenses/by/4.0/>).

Abstract: The present work proposes an experimental strategy to prepare argan nutshell-derived porous carbons using potassium hydroxide (KOH). Several experimental parameters of the activation process were evaluated (temperature, impregnation ratio, and activation time), and an optimized carbon (ACK) was obtained. The surface properties of the ACK sample were determined, and the porous carbon was applied as an adsorbent of diclofenac (DCF) and paroxetine (PARX). A commercial carbon (CC) was used as a benchmark. The ACK porous carbon presented a higher surface area and micropore volume ($1624 \text{ m}^2 \text{ g}^{-1}$ and $0.40 \text{ cm}^3 \text{ g}^{-1}$, respectively) than CC carbon ($1030 \text{ m}^2 \text{ g}^{-1}$ and $0.30 \text{ cm}^3 \text{ g}^{-1}$, respectively), but the maximum adsorption capacities of DCF ($214\text{--}217 \text{ mg g}^{-1}$) and PARX ($260\text{--}275 \text{ mg g}^{-1}$) were comparable among the two carbons. Besides $\pi\text{--}\pi$ interactions, H-bonds with the electronegative atoms of the adsorbate molecules and the electropositive H of the oxygen functional groups were appointed as the most probable mechanisms for adsorption onto ACK porous carbon. The electrostatic attraction was also considered, particularly for DCF with CC carbon. The pore size might have also been critical, since CC carbon presented more supermicropores ($0.7\text{--}2 \text{ nm}$), which are usually more favorable toward the adsorption of pharmaceutical molecules. The reusability of the ACK carbon was tested up to four cycles of adsorption–desorption by using ultrasonic washing with water. The results indicated that no more than one cycle of use of ACK should be performed.

Keywords: argan nutshells; waste valorization; porous carbon; adsorption; water treatment

1. Introduction

Activated carbon (AC) is considered a highly efficient adsorbent with major industrial significance due to its high surface area, tunable surface chemistry, and a high degree of surface reactivity [1–3]. These excellent properties make it possible to use these materials in several applications, including water treatment, gas storage, catalyst support, energy storage,

medicinal uses, biomedical engineering, and metal recovery, among others [4–6]. For these applications, porous carbons prepared from several low-cost renewable feedstocks, such as agroforestry wastes/by-products, have been used [4,7]. Hard-shelled agricultural wastes constituted good precursors for porous carbons due to their high contents of lignin [4,8]. Argan nutshells, generated after extracting the argan oil from the kernels of the Argan tree (*Argania spinosa*), are available in huge amounts every year, since argan oil is widely used within the international oils market due to its beneficial properties in therapeutic medicine, cosmetic, and the culinary arts [9–11]. The Argan tree grows extensively across Northwest Africa, particularly in Algeria, especially in the Tindouf region [12]. Thus, the sustainable valorization of biomass wastes resulting from the production of the argan oil into new products in the concept of circular economy has the potential to make a positive socioeconomic impact on this region. Although the nutshell of argan fruit is mostly used by locals for heating, efforts have been made for the conversion of argan nutshells into added-value products, namely adsorbents [13], biocomposite materials [14,15], and porous carbons [16,17]. The high lignin content (around 35% *w/w*) and the low ashes content (<1% *w/w*) of argan nutshells [14] have allowed the production of high-quality carbons with a highly developed porous structure and well-defined pore size distribution, desirable properties for energy storage [16,18,19], and adsorption applications [17,20,21]. Nevertheless, the use of argan nutshell-derived porous carbons as adsorbents still falls short and has been focused mainly on the adsorption of bisphenol and diuron [17,21,22].

Emerging contaminants (ECs), such as pharmaceutical compounds, are being detected worldwide in different water bodies, posing a significant risk to the aquatic environment and raising attention to this increasing problem [23,24]. In fact, wastewater treatment plants (WWTPs) cannot completely remove some of these ECs, leading to their discharge in the receiving aquatic compartments [25]. Among the advanced treatments used in WWTPs directed to remove micropollutants, adsorption by activated carbons is considered simple, low-cost, not producing harmful by-products, reusable, efficient, and safe when compared to membrane processes, reverse osmosis, and advanced oxidation processes [24,26]. Moreover, it can be easily integrated with other treatments [26].

Considering all the above, the present work proposes a strategy to prepare argan nutshell-derived porous carbons via chemical activation using potassium hydroxide (KOH). The valorization of argan nutshells, an undervalued waste, into high added-value adsorbents can significantly impact the rural communities that strongly depend on the argan oil economy. Several experimental parameters of the activation process were tested and evaluated to obtain an optimized porous carbon. The porous carbon was thoroughly characterized and applied as an adsorbent of diclofenac (DCF) and paroxetine (PARX) present in water. These two compounds represent ECs from the nonsteroidal anti-inflammatory (NSAI) and antidepressant groups, respectively, which are two pharmaceutical classes frequently detected in wastewaters. Moreover, DCF is one of the most used painkillers and NSAI drugs around the world with proven toxicity at low concentrations for aquatic life and human health. Its high recalcitrance level led to frequent detection in wastewaters [27]. PARX consumption has increased in the last years, already detected in aquatic organisms [28], but its removal through adsorption still lacks knowledge. The removal of these compounds and the development of highly efficient adsorbents for their adsorption is, therefore, of utmost importance.

This work constitutes a follow-up to a previous work where H_3PO_4 activation was performed on argan nutshell wastes [29]. In the present work, the properties and performance of alkali-activated carbon were compared to the acidic ones.

2. Materials and Methods

2.1. Raw Materials

The shells obtained from argan nuts (ANS) were grounded and sieved to particle sizes between 0.5 mm and 1.6 mm. The particles were rinsed with water and then dried at 75 °C

in an oven for 3 days. The characterization of the ANS waste was performed in a previous work [29].

2.2. Porous Carbons Synthesis

The series of activated carbons prepared from ANS followed a strategy of two steps: carbonization (step 1), followed by chemical activation with KOH (step 2). Carbonization and activation were carried out by using a tubular Carbolite 2416 furnace in a horizontal configuration with an alumina reactor. In the first step, the ANS was carbonized at 400 °C (heating rate of 5 °C min⁻¹) for 1 h under a N₂ flow (around 100 cm³ min⁻¹) and then cooled to room temperature, always under N₂ atmosphere. The second step consisted of the dry impregnation of the carbonized product (biochar) with KOH.

In the activation process, the biochar was first impregnated with KOH and then carbonized under an N₂ flow of 100 mL min⁻¹ by varying the following parameters, in this order: (1) activation temperature, (2) impregnation mass ratio, and (3) activation time. The heating rate was constant in all the activation assays, 5 °C min⁻¹.

After each activation experiment, the obtained carbons were mixed with a HCl solution (0.1 mol L⁻¹) and boiled for 3 h under reflux. The solution was filtered, and the carbon was rinsed with hot water until no chloride ions were detected in the washing water (AgNO₃ test). The washed carbon was subsequently dried overnight at 70 °C.

Table 1 summarizes the experimental design used to synthesize the KOH-activated samples.

Table 1. Experimental design for porous carbons synthesis and nomenclature of samples.

Sample Name	Temperature (°C)	Activation Time (h)	Biochar:KOH Mass Ratio
Temperature effect			
ACK700_1_1:1.5	700	1	1:1.5
ACK800_1_1:1.5	800	1	1:1.5
Mass ratio effect			
ACK800_1_1:1	800	1	1:1
ACK800_1_1:1.5	800	1	1:1.5
ACK800_1_1:2	800	1	1:2
Activation time effect			
ACK800_1_1:2	800	1	1:2
ACK800_2_1:2	800	2	1:2

2.3. Porous Carbons Characterization

The obtained carbons were submitted to N₂ adsorption–desorption isotherms at −196 °C (Micromeritics ASAP 2010 equipment, Atlanta, GA, USA) for evaluating their surface area and pore volume. Specific surface areas, S_{BET} (BET method), micropore volume, V_{Mic} (t-plot method), and total pore volume, V_T (N₂ adsorption at p/p₀ = 0.95) were determined. The mesopore volume (V_{Mes}) was calculated from V_T − V_{Mic}. The micropore size distribution was determined with the density functional theory (DFT) (adsorption model for carbon slit-shaped pores), and the mesopore size distribution was determined by using the BJH method. From these results, the carbon with the higher porosity was selected. This carbon sample, coded as ACK, and the commercial carbon, CC, were submitted to additional characterizations:

1. Elemental analysis—Quantification of C, H, N, and S (Thermo Finnigan-CE Instruments Flash EA 1112 CHNS analyzer, Waltham, MA, USA);
2. Ash content—Residue after combustion at 750 °C for 6 h in a muffle furnace (ASTM D1762);
3. pH at the point of zero-charge (pH_{PZC})—A series of 6 solutions of NaCl (0.01 mol L⁻¹, 20 mL) was prepared, and the pH of each solution was adjusted in the range of 2–12 by adding 0.1 M NaOH or 0.1 M HCl. Then, 0.05 g of the carbon was added to

- each solution, agitated for 48 h, and the final pH of each solution was measured. The pH_{PZC} was obtained from the plot of pH_{drift} versus $\text{pH}_{\text{initial}}$;
4. Thermogravimetric analysis (TGA)—Mass loss between 30 and 900 °C (heating rate of 5 °C min⁻¹) under argon atmosphere (Setaram Labsys EVO, France);
 5. Fourier-Transform Infrared Spectroscopy (FTIR)—KBr disk method (Perkin-Elmer Spectrum 1000 Spectrometer, Waltham, MA, USA) in the range of 400–4000 cm⁻¹ (resolution of 1 cm⁻¹);
 6. X-ray Photoelectron Spectroscopy (XPS)—XPS of the carbon surface was obtained by using the Mg K α radiation ($h\nu = 1253.6$ eV) from an XSAM800 dual anode spectrometer from Kratos. The operation conditions of the XPS analysis were as described in [30]. The detailed regions C 1s, O 1s, N 1s, and S 2p were acquired;
 7. Temperature programmed desorption (TPD)—100 mg of each sample was heated to 1100 °C (heating rate of 5 °C min⁻¹) under a flow rate of 25 cm³ min⁻¹ of He. The profiles of CO and CO₂ were obtained with automated AMI-300 equipment (Altamira Instruments) connected to a mass spectrometer (Dymaxion 200, Ametek, PA, USA). Quantification of CO and CO₂ released through calibration at the end of each experiment;
 8. Scanning Electron Microscopy with Energy Dispersive Spectroscopy (SEM-EDS)—The morphology and elemental composition of ACK were obtained by using a JEOL 7001F analytical FEG-SEM equipment with an energy-dispersive X-ray spectrometer light element detector attachment.

2.4. Batch Adsorption Studies

The granulometry of both ACK and CC used in the adsorption assays was 50–70 mesh. DCF standard solution with a concentration of 1000 mg L⁻¹ was prepared by dissolving diclofenac sodium salt (Alfa Aesar, Haverhill, MA, USA, 98%) in deionized water, and the solutions used in the adsorption assays were obtained from a dilution of the standard. PARX aqueous standard solution with a concentration of 100 mg L⁻¹ was prepared from paroxetine hydrochloride extracted from a commercial drug, and subsequent working solutions were prepared from a dilution of the standard. The molecular structures of the adsorbates are presented in Figure S1 (Supplementary Materials).

The adsorption of the pharmaceutical compounds onto ACK and CC in batch mode was investigated through kinetics and equilibrium studies by stirring 10 mg of adsorbent with 25 mL of adsorbate solution at 200 rpm in an orbital shaker. The effect of the solution pH on the uptake of DCF and PARX was also assessed by adjusting the initial pH of the solutions in the range of 6–10 for DCF and from 5–9 for PARX. The studied pH ranges were based on the stability and solubility of the molecules and on carbon's surface charge [29]. The solutions used in the pH study presented a concentration of 100 mg L⁻¹ and pH values of 6.0 and 5.5 for DCF and PARX, respectively. A contact time of 24 h and an initial adsorbate concentration of 100 mg L⁻¹ were used in these assays. Kinetic tests were carried out from 5 min until 1440 min (24 h). Equilibrium experiments (adsorption isotherms) were performed by using solutions with concentrations from 20 to 200 mg L⁻¹. The temperature effect on DCF and PARX adsorption was evaluated between 298 and 323 K (25–50 °C) by using an initial concentration of 100 mg L⁻¹ of each adsorbate. Blank tests and duplicates were performed.

The concentrations of each adsorbate after each adsorption assay (and after filtration) were determined by UV–Vis spectrophotometry (GBC UV/VIS, model 916, Hampshire, MA, USA) by using a wavelength of 274 and 293 nm for DCF and PARX, respectively. The calibration curves for each compound were determined.

The adsorption capacity of DCF and PARX, q_t (mg g⁻¹), and their removal efficiency, η (%), were determined according to Equations (1) and (2):

$$q_t = \frac{(C_0 - C_f) \times V}{m} \quad (1)$$

$$\eta = \frac{(C_0 - C_f) \times 100}{C_0} \quad (2)$$

C_0 , initial concentration (mg L^{-1}); C_f final concentration (mg L^{-1}); V , volume of the solution (L); m , mass of adsorbent (g).

2.5. Desorption Studies

To evaluate the efficiency of the optimized biomass-derived carbon, regeneration cycles of ACK samples saturated with DFC and PARX were performed by using the ultrasonic technique. Desorption tests were carried out using an ultrasonic equipment ARGO LAB model AU-32, at 40 kHz and 100 W.

At first, the adsorption process was carried out as described before, with 0.1 g of ACK carbon added to 250 mL of the DFC and PARX solutions with an initial concentration of 100 mg L^{-1} in flasks. The flasks were stirred at 200 rpm at room temperature until the equilibrium was reached. At the end of the adsorption process, the concentrations of DFC and PARX in the solutions were determined by UV-Vis.

The desorption assays were carried out by separating the adsorbent from the solution by filtration, and then the loaded adsorbent was added to 100 mL of deionized water. The samples were placed in an ultrasonic bath for 30 min. The mixture was then filtrated, and 100 mL of more fresh deionized water was added and again sonicated for an additional time of 30 min. After each regeneration step, the adsorbent was kept in the oven overnight at 70°C . Four regeneration cycles were performed.

At the end of each regeneration cycle, an adsorption assay was performed again under the same conditions described above. All the experiments were carried out in duplicate.

3. Results and Discussion

The textural properties of the obtained porous carbons were evaluated to select an optimized carbon to be thoroughly characterized. The selected carbon and a benchmark material were then applied to the adsorption of DCF and PARX and their performances compared.

3.1. Porous Carbons Characterization

3.1.1. N_2 Adsorption-Desorption Isotherms and Pore Size Distribution

The textural parameters obtained from the N_2 adsorption-desorption isotherms are shown in Table 2.

Table 2. Textural parameters of carbons obtained from the N_2 adsorption-desorption isotherms.

Sample Name	S_{BET} ($\text{m}^2 \text{g}^{-1}$)	V_{T} ($\text{cm}^3 \text{g}^{-1}$)	V_{Mic} ($\text{cm}^3 \text{g}^{-1}$)	V_{Mes} ($\text{cm}^3 \text{g}^{-1}$)
Biochar	<5.0	-	-	-
CC ^a	1030	0.56	0.30	0.26
ACK700_1_1:1.5	1063	0.51	0.25	0.26
ACK800_1_1:1.5	1542	0.76	0.33	0.43
ACK800_1_1:1	1214	0.45	0.37	0.08
ACK800_1_1:2	1624	0.74	0.40	0.34
ACK800_2_1:2	678	0.35	n.d.	n.d.

^a [29]; S_{BET} —specific surface area; V_{T} —total pore volume; V_{Mic} —micropore volume; V_{Mes} —mesopore volume.

As expected, the biochar sample presented an extremely low specific surface area ($<5 \text{ m}^2 \text{g}^{-1}$) caused by the blocking of tarry substances produced in the pyrolysis process [31,32]. The strategy of producing first the biochar and then impregnating it with the activation agent has the proven advantage of improving the surface area and pore size distribution in the resulting activated carbon with less consumption of the chemical agent, since KOH diffuses more easily into the char matrix to react with the carbon atoms [33,34]. Although the two-stage approach increases the energetic consumption of the process, it is balanced with the higher surface areas of the resulting carbons, as well as a fine development of the porosity. Thus, the textural properties of the activated biochar were significantly improved after KOH activation. The mechanism of KOH

activation for porosity formation was already described: a redox reaction catalyzed by alkali metal occurs, where the carbon atoms are oxidized to CO or CO₂; then, the reduced alkali metal is intercalated between the graphene layers, expanding the carbon structure [35,36].

The produced carbons presented surface areas higher than the commercial carbon, which constitutes a very interesting result. However, sample ACK800_2_1:2 presented a much lower surface area (678 m² g⁻¹), indicating that 2 h of activation was excessive and promoted some collapse of the pores. As presented in Table 2, the activation temperature has a significant impact on the surface area, allowing the development of more micropores and mesopores at 800 °C. Additionally, the KOH impregnation ratio has an impact on the textural properties, since the higher Biochar:KOH mass ratio (1:2) provided an activated carbon with the highest surface area.

According to these results, the sample impregnated with Biochar:KOH in a 1:2 ratio and activated at 800 °C for 1 h was selected for further characterization and application in the adsorption assays, given its advanced porosity and higher surface area. From this point onwards, this sample will simply be called ACK. A comparison between ACK carbon and CC commercial carbon was investigated.

Figure S2 (Supplementary Materials) gives the N₂ adsorption isotherms of the ACK and CC samples. ACK carbon presents a type I (b) isotherm, while CC carbon shows mixed type I and IV isotherms [29]. The higher volume of adsorbed N₂ of the ACK sample agrees with the higher surface area of this carbon. The type I (b) isotherm is associated with microporous materials presenting micropore size distributions over a broad range, including wider micropores and narrow mesopores (<2.5 nm), whereas the type IV isotherm indicates both micro- and mesoporous structures, according to the IUPAC classification [37]. The larger hysteresis loop of CC isotherm indicates larger mesopores in this sample.

Figure 1 displays the PSD of ACK and CC carbons.

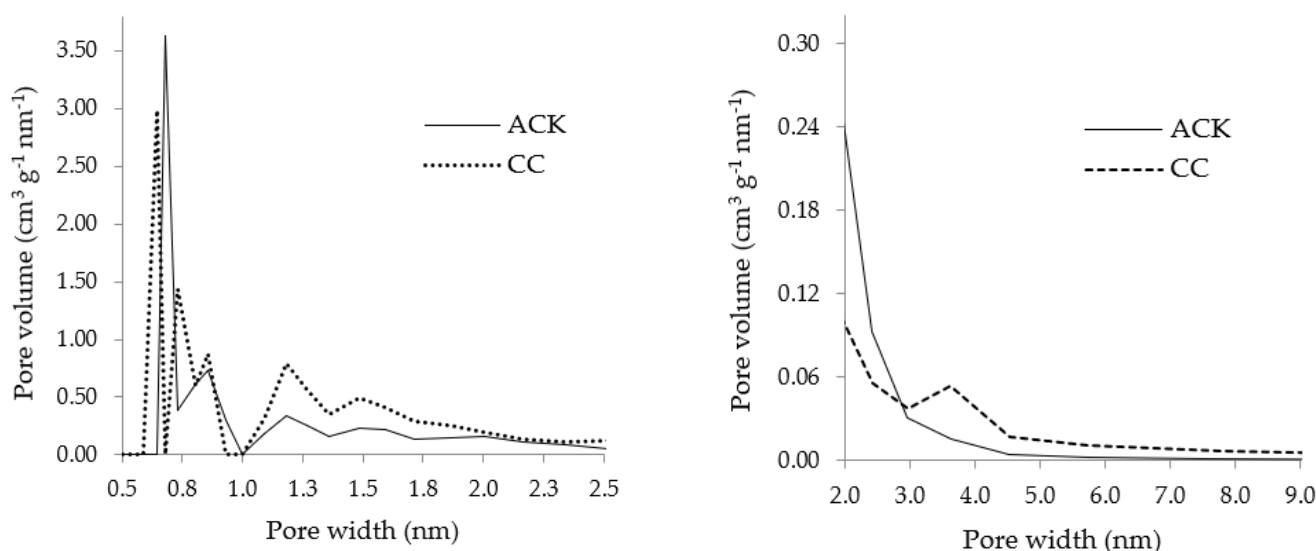


Figure 1. Micropore size distribution (DFT adsorption model for carbon slit-shaped pores) (left) and mesopore size distribution (BJH method) (right) of the carbon samples.

The micropore size distribution displays that both carbons presented a well-developed microporous structure with a dominance of pore widths between 0.6 and 0.7 nm. Between 0.7 and 2.0 nm, the pore size distribution is similar for both carbons, although it seems that CC carbon is richer in micropores with this size range. The mesopore size distribution from the BJH model shows that both carbons also show a broad distribution of mesopores, but ACK carbon presents mainly small mesopores (<3.0 nm) while CC carbon has a predominance of mesopores with pore widths between 3.0 and 4.5 nm.

3.1.2. Elemental Analysis and Ash Content

Table 3 presents the elemental analysis and ash content of ANS biomass [29], ANS-derived biochar, ACK, and CC carbons, as well as the pH_{PZC} of carbons.

Table 3. Elemental analysis and ash content of the ANS, Biochar, ACK, and CC samples.

	ANS ^a	Char	ACK	CC ^a
C (wt.%)	47.8	74.6	69.9	86.3
H (wt.%)	6.54	3.44	1.74	0.47
N (wt.%)	0.33	0.30	0.39	<0.20
S (wt.%)	<0.03	<0.03	0.20	0.57
O ^b (wt.%)	45.2	21.4	26.9	6.76
Ashes (wt.%)	0.065	0.26	0.95	5.70
pH_{PZC}	-	-	7.0	9.1

^a [29]; ^b Calculated by difference (wt. %): $100 - (\text{C} + \text{H} + \text{N} + \text{S} + \text{Ash})$.

The ANS composition was published before [29], highlighting the very low ash content in this biomass. Thus, the resulting biochar and ACK porous carbon from ANS also presented a low ash content. As expected, the amount of elemental carbon increased after the ANS pyrolysis from 47.8 to 74.6 wt%, while the oxygen content decreased significantly from 45.2 wt% to 21.4 wt%. After the chemical activation of the biochar with KOH, the carbon content of the resulting carbon ACK decreased slightly, but the oxygen content increased from 21.4 wt% to 26.9 wt%, suggesting that the KOH treatment increased the amount of oxygen functional groups a little bit. Nevertheless, ACK carbon presented a neutral pH_{PZC} ; thus, the oxygen surface functional groups must be nonacidic. On the other hand, CC carbon showed a higher amount of C and ashes but lower O content compared to ACK carbon. As previously demonstrated [29], this commercial carbon presented a basic nature.

3.1.3. Thermogravimetric Analysis (TGA)

Figure S3 (Supplementary Materials) displays the TGA curves for the ANS raw material, carbonized ANS (Biochar), and ACK and CC carbons. The thermal profile of the ANS biomass was previously presented and discussed [29]. A major weight loss between 230 and 400 °C can be observed and for the remaining 25% (*w/w*) of the initial mass of biochar material at 850 °C.

The TGA curve for the biochar sample showed a weight loss of around 20% (*w/w*) in the temperature range of 400–600 °C, corresponding to the decomposition of the residual organic matter. ACK carbon presented thermal stability up to 600 °C (weight loss of 10%, *w/w*). From there on, an accentuated weight loss was observed up to 900 °C, attributed to a possible decomposition of minerals retained in the carbon matrix and/or to the decomposition of the surface functional groups. CC carbon presented a stable temperature profile, as shown in Figure S3 (Supplementary Materials), with a weight loss of 7% (*w/w*) up to 900 °C.

3.1.4. FTIR Analysis

Figure 2 depicts the 400–4000 cm^{-1} infrared spectral region of the carbon samples.

The FTIR spectrum of argan nut shells [29] showed strong bands attributed to stretching vibrations of the hydroxyl groups (O-H) of phenols/alcohols, strong bands associated with the stretching of carbonyl groups (C=O) and of the C-O stretch vibration of the alcohols or ethers. The profile of the FTIR spectra of the activated carbon samples reveals, as expected, and a considerable reduction in the intensity or even the disappearance of some bands ascribed to several functional groups removed during the high temperatures of the activation process. In the case of the biochar, it is possible to observe a few bands with relevant intensities, most of them related to the aromatization of the carbon matrix during carbonization: bands at 1580 and 1430 cm^{-1} assigned to C=C aromatic ring stretch and

bands at 750 and 815 cm^{-1} associated with the aromatic C-H out-of-plane bend [38]. There are common bands among the activated carbon samples—namely, the band at 1385 cm^{-1} attributed to the O-H bend frequency of phenol, the bands at 1622–1633 cm^{-1} associated with C=O groups and, also, to C=C aromatic ring stretching vibrations, and the bands at 1132–1180 cm^{-1} , usually assigned to the C–O stretch vibration of alcohols or ethers.

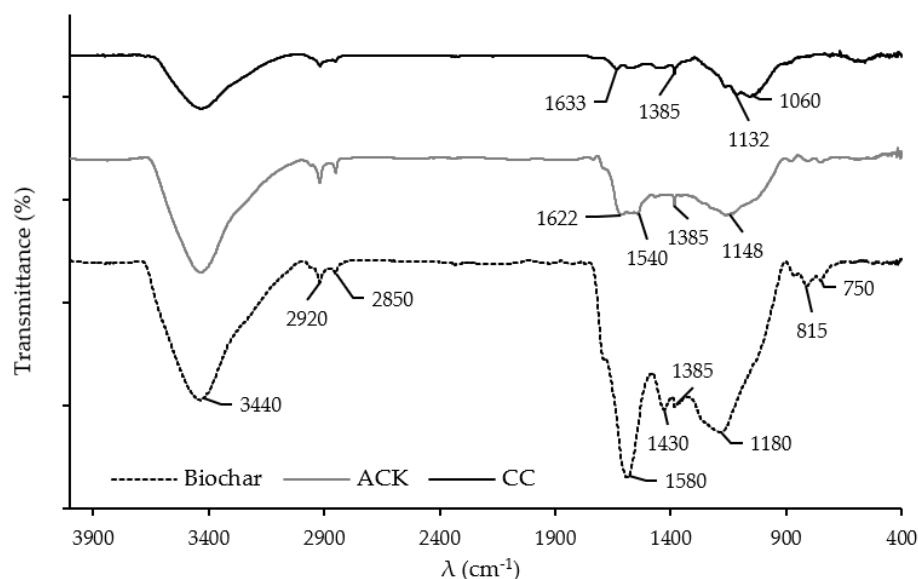


Figure 2. FTIR spectra of char and the ACK and CC porous carbons.

3.1.5. XPS Analysis

To get further insight into the surface chemistry of the carbons, XPS analyses were performed. Two distinct peaks (C 1s and O 1s) were observed in the XPS survey scan of the ACK and CC carbons; therefore, the C 1s and O 1s XPS detailed regions were acquired (Figure S4 of the Supplementary Materials), and the corresponding data are presented in Table 4.

Table 4. Binding energy values (eV) for C 1s and O 1s fitted peaks, atomic concentrations %, and atomic ratios.

CC	ACK	CC ^a	ACK	Assignment [39]
Binding Energy (eV)		Atomic Concentration %		
284.8	284.8	66.5	55.0	C _{arom} + C _{aliph}
286.2	286.2	11.5	15.9	C–O
287.4	287.6	6.3	7.8	C=O
288.9	289.0	3.8	4.4	O–C=O
290.2	290.5	3.1	3.1	
291.7	292.1	2.6	1.7	$\pi \rightarrow \pi^*$
530.8	531.0	0.8	1.7	C=O _{arom}
532.1	532.4	1.8	3.7	C=O _{alif}
533.2	533.8	2.0	2.7	C–O
534.6	535.4	0.9	1.2	Isolated H ₂ O
536.0	537.0	0.7	0.7	H ₂ O
Atomic ratio		14.1	8.3	C/O
		6.0	5.5	$\pi \rightarrow \pi^*/\text{Ctotal}$

^a [29].

The C 1s XPS regions were fitted with six peaks. The most intense peak on both carbons was positioned at 284.8 eV, attributed to a mixture of aromatic and aliphatic carbon. The peaks centered at around 286.2 eV were assigned to C–O of the ether or alcohol groups, this functional group being dominant in both carbons. The peaks appearing between 287 and 289 eV corresponded to carbon in the carbonyl (C=O) and carboxyl (–COOH)

functional groups. The region between 290 and 292 eV corresponded to energy losses due to $\pi \rightarrow \pi^*$ electronic excitations typical of aromatic systems. Meanwhile, the O 1s region was peak-fitted with five peaks with binding energies from 530 to 536 eV, confirming the presence of the oxidized carbonaceous species and some water.

From Table 4, through the C/O ratio, it is possible to observe that ACK carbon presented more oxygenated surface functional groups than commercial carbon.

3.1.6. TPD Analysis

The amounts of CO and CO₂ evolved in the TPD experiments were also measured to understand the nature of the carbon surface groups. CO₂ evolution results from the decomposition of carboxylic acids at $T < 450$ °C and lactones at higher temperatures, $550 < T < 800$ °C; carboxylic anhydrides originate in both CO and CO₂ at intermediate temperatures, $400 < T < 600$ °C; phenols decompose into CO at intermediate temperatures, $550 < T < 800$ °C; and carbonyl-quinone groups release CO at high temperatures, $750 < T < 1100$ °C [40]. Figure S5 (Supplementary Materials) displays the TPD spectra for both carbons. Table 5 presents the results of the deconvolution of TPD spectra using a multiple Gaussian function, as well as the amounts of CO and CO₂ released obtained by integration of the areas under the TPD peaks.

Table 5. Results of the deconvolution of CO₂ and CO spectra using a multiple Gaussian function.

Sample	Carboxylic Acids			Carboxylic Anhydrides			Lactones			Total CO ₂ (±20 $\mu\text{mol g}^{-1}$)
	T _m (°C)	W (°C)	A ($\mu\text{mol g}^{-1}$)	T _m (°C)	W (°C)	A ($\mu\text{mol g}^{-1}$)	T _m (°C)	W (°C)	A ($\mu\text{mol g}^{-1}$)	
ACK	278	200	308	138	172	191	655	172	234	738
CC ^a	220	219	179	498	242	126	754	242	99	390

Sample	Carboxylic Anhydrides			Phenols			Carbonyls or Quinones			Total CO (±20 $\mu\text{mol g}^{-1}$)
	T _m (°C)	W (°C)	A ($\mu\text{mol g}^{-1}$)	T _m (°C)	W (°C)	A ($\mu\text{mol g}^{-1}$)	T _m (°C)	W (°C)	A ($\mu\text{mol g}^{-1}$)	
ACK	469	172	191	641	151	482	802	151	582	1291
CC ^a	498	242	126	673	154	211	859	154	329	695

^a [29]; T_m—temperature of the peak maximum; W—width of the peak at half-height; A—integrated peak area.

Overall, ACK carbon presented higher amounts of CO and CO₂ released, confirming the results of the elemental and XPS analyses that indicated the presence of more oxygen functional groups at this carbon's surface. Additionally, the amount of CO released was higher than that of CO₂ for both samples, indicating that the oxygen groups present in the carbons were mainly nonacidic (carbonyl and quinone groups), in agreement with the pH_{PZC} of these carbons (Table 3). Effectively, as indicated by the TPD results, the main surface functional groups in both carbons are phenols and carbonyls/quinones.

3.1.7. SEM-EDS

Figure 3 presents the surface morphology of an ACK particle and the EDS spectrum.

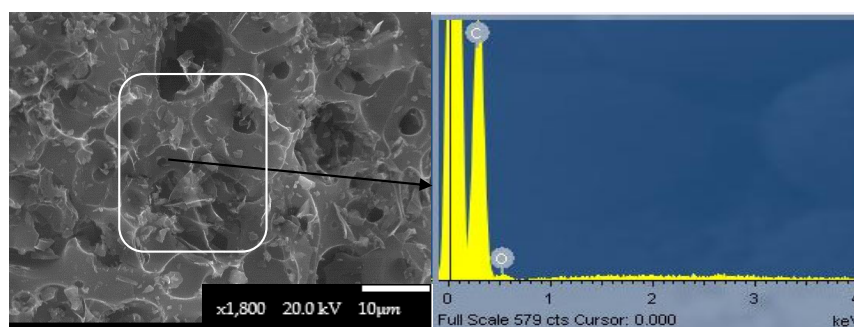


Figure 3. SEM image of ACK carbon with a magnification of 1800 \times and the corresponding EDS spectrum.

The SEM image showed that the external surface of ACK contains many cavities that are formed from the evaporation of the products resulting from the reactions of KOH activation [41]. In contrast, the CC particles presented a rough surface with no cavities visible (Figure S6 of the Supplementary Materials). The EDS spectrum of the ACK particle showed that the dominant elements were carbon and oxygen, which agrees with the elemental analysis, while the EDS spectrum of the CC particle also revealed the presence of other elements such as Al, Si, S, and Ca (Figure S6 of the Supplementary Materials).

3.2. DCF and PARX Adsorption Assays

3.2.1. Effect of Initial pH

The effect of the solution pH on the adsorption process is known as an important operating parameter. Figure 4 shows the effect of the solution pH on the adsorption of DCF and PARX.

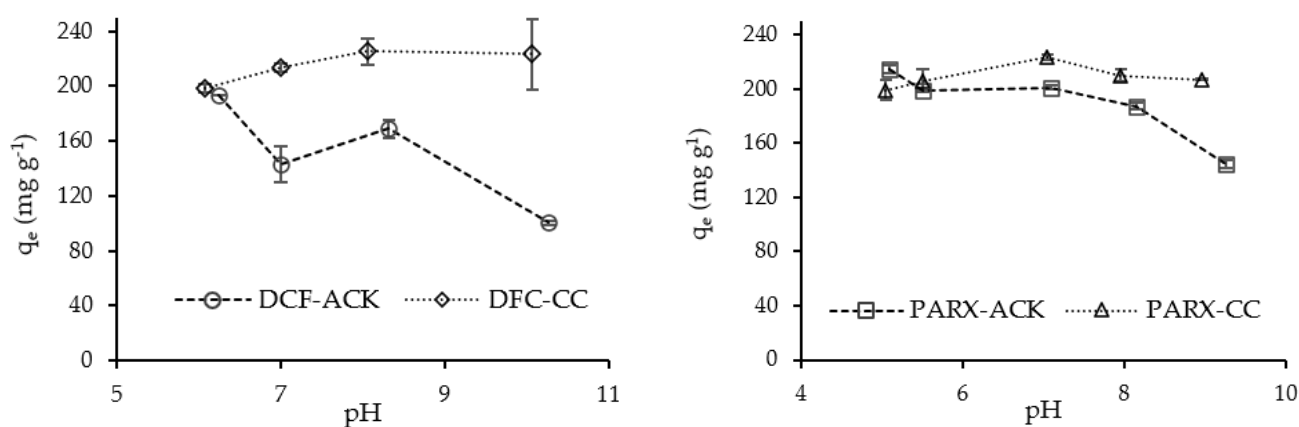


Figure 4. Effect of solution pH on the uptake capacity of DCF and PARX for ACK and CC carbons. (Adsorbent mass = 10 mg; DCF and PARX initial concentration = 100 mg L⁻¹; solution volume = 25 mL; contact time = 24 h).

It is possible to observe a decrease in the adsorption capacity of DCF with ACK carbon with the increase of pH. According to the pH_{PZC} value of ACK (Table 3), this carbon acquired negative charges for pH values above 7.0, while the DCF molecule is in an anionic form in the pH range studied [42], which means that electrostatic repulsion occurs with the increasing pH. CC carbon presents a positively charged surface below its pH_{PZC} (9.13), attracting the DCF molecule through electrostatic interactions, justifying the higher uptake capacity of this carbon for DCF. However, for the sake of simplicity and comparison purposes, the DCF solution was used without pH adjustment for the next adsorption assays with both carbons.

The PARX molecule presents a basic nature, and it is protonated in the studied pH range [29], with a positive net charge attributed to the N-H₂ group [43], to observe a decrease in its uptake capacity for ACK carbon being possible, particularly for pH values above the pH_{PZC} value of carbon (7.0). Somehow, the negatively charged surface of ACK presented a decreased affinity to the PARX molecule.

On the other hand, the adsorption capacity of PARX onto CC carbon was not affected by the solution pH. Although both porous carbon and molecule presented positive charges, electrostatic repulsion was surpassed by another adsorption mechanism.

Given these results, the PARX solution was used in the subsequent assays without a pH adjustment.

3.2.2. Kinetic Study

The effect of time (kinetic assay) was studied for the adsorption of both drugs (Figures 5 and 6).

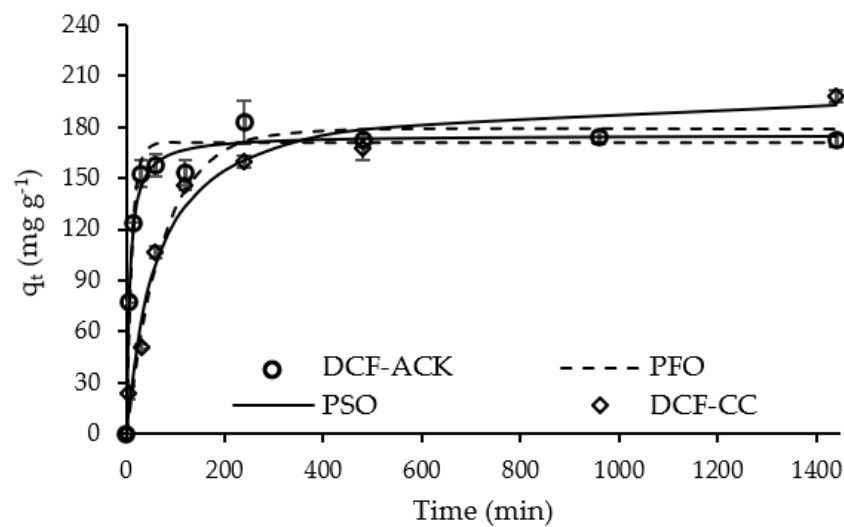


Figure 5. Kinetic curves of DCF adsorption for ACK and CC carbons (Adsorbent mass = 10 mg; DCF initial concentration = 100 mg L⁻¹; Solution volume = 25 mL; Solution initial pH = 6.00). Dots—experimental data; Lines—kinetic model adjustments.

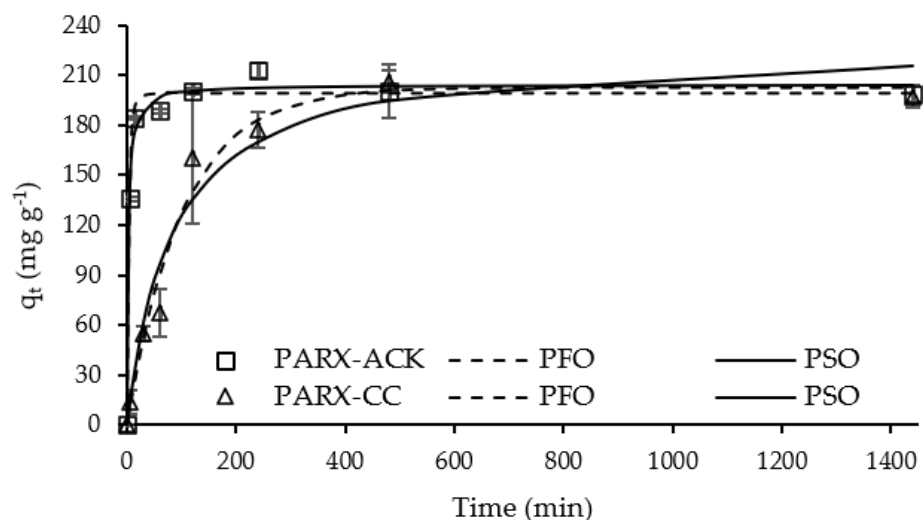


Figure 6. Kinetic curves of PARX adsorption for ACK and CC carbons (Adsorbent mass = 10 mg; PARX initial concentration = 100 mg L⁻¹; Solution volume = 25 mL; Solution initial pH = 5.5). Dots—experimental data; Lines—kinetic models' adjustment.

DCF and PARX uptake by ACK carbon achieved equilibrium at 240 min (4 h), with adsorption capacities of 182 mg g⁻¹ and 212 mg g⁻¹, respectively. On the other hand, the adsorption of both molecules by CC carbon reached equilibrium at around 480 min (8 h), indicating a slower adsorption rate. The adsorption capacities of DCF and PARX at equilibrium with CC carbon were 167 mg g⁻¹ and 205 mg g⁻¹, respectively, quite comparable to the values obtained at equilibrium for ANS-derived carbon. Thus, despite the higher surface area and micropore volume of ACK carbon (Table 2), its uptake capacity was not significantly higher than the one obtained for the commercial adsorbent.

Experimental data were adjusted to the pseudo-first-order (PFO) and pseudo-second-order (PSO) kinetic nonlinear models [44,45] (Table S1, Supplementary Materials) through the minimum of the least-squares method. The best-fitting model was chosen based on the determination coefficient, R². The kinetic parameters obtained from the models are presented in Table 6.

Table 6. Kinetic parameters obtained from the adjustment of the PFO and PSO models to the experimental kinetic data.

	DCF		PARX	
	ACK	CC ^a	ACK	CC ^a
<i>PFO model</i>				
R ²	0.972	0.976	0.989	0.980
q _e (mg g ⁻¹)	171	179	199	202
k ₁ (min ⁻¹)	0.095	0.013	0.222	0.010
<i>PSO model</i>				
R ²	0.986	0.983	0.992	0.960
q _e (mg g ⁻¹)	175	201	204	227
k ₂ (g mg ⁻¹ min ⁻¹)	9 × 10 ⁻⁴	1 × 10 ⁻⁴	0.002	5 × 10 ⁻⁵

q_e—Amount of adsorbate uptake per mass of adsorbent at equilibrium; k₁—PFO rate constant; k₂—PSO rate constant; R²—determination coefficient; ^a [27].

Both kinetic models were well-fitted to the experimental data (R² > 0.900), although the PSO kinetic model presented the best fit to most of the drug-carbon systems, with an exception for the PARX-CC system that presented a slightly better adjustment for the PFO model. Although these kinetic models are essentially mathematical and constituted by empirical equations, some authors mentioned that a good fit to the PFO model indicates that the surface reaction acts as the rate-limiting step, while the PSO model generally implies that the rate of adsorption is limited by the process of diffusion into a network of small pores [46,47].

It can be observed that the kinetic constant values are higher for the systems with the ACK sample, confirming the faster uptake of the molecules by this carbon due to its higher mesopore volume (Table 2). The uptake of PARX onto ACK carbon is the fastest, probably due to a higher affinity of the molecule to the adsorption sites of this carbon, as discussed further ahead (Section 3.2.4).

Based on these results, an equilibrium time of 4 h has been chosen to complete the adsorption studies with ACK carbon for both drugs. For CC carbon, the equilibrium time chosen for both pharmaceutical compounds was 8 h.

3.2.3. Adsorption Equilibrium Studies

Figures 7 and 8 present the adsorption equilibrium curves of DCF and PARX for ACK and CC carbons.

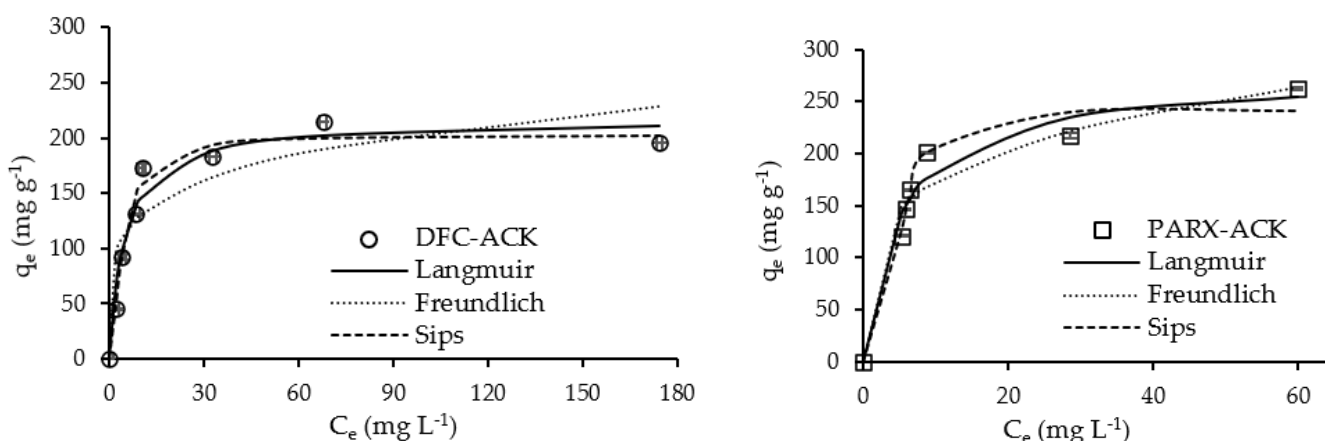


Figure 7. Adsorption equilibrium curves of DCF and PARX for ACK carbon (Adsorbent mass = 10 mg; Contact time = 4 h; Solution volume = 25 mL; Solution initial pH = 6.0 (DCF) and 5.5 (PARX)). Dots—experimental data; Lines—isorthem models’ adjustment.

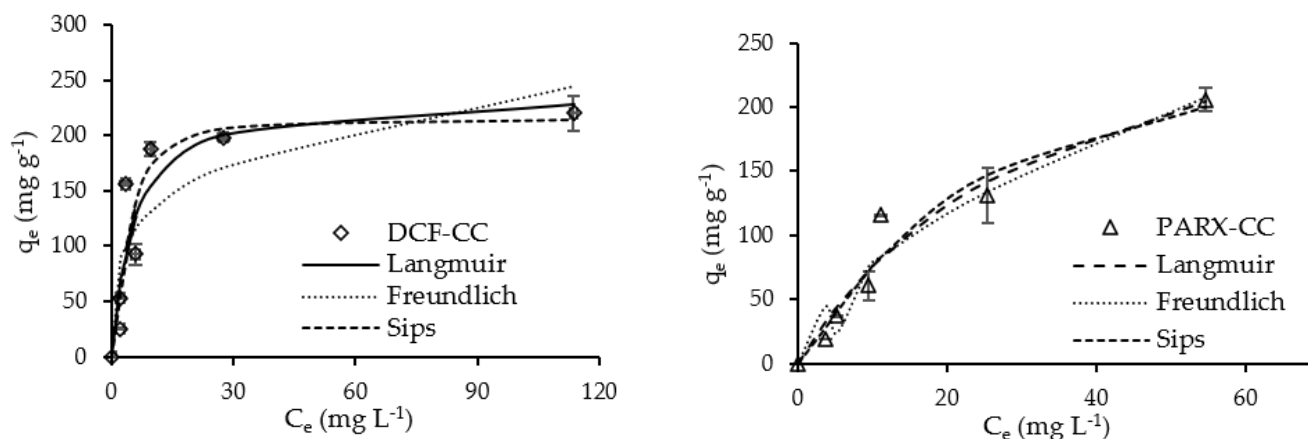


Figure 8. Adsorption equilibrium curves of DCF and PARX for CC carbon (Adsorbent mass = 10 mg; Contact time = 8 h; Solution volume = 25 mL; Solution initial pH = 6.0 (DCF) and 5.5 (PARX)). Dots—experimental data; Lines—isorthem models’ adjustment.

The experimental data were modelled with the Langmuir, Freundlich, and Sips nonlinear models [48–51] through the minimum of the least-squares method, and the best-fitting model was chosen through the highest determination coefficient, R^2 . The model parameters obtained from the adjustments are presented in Table 7, observing that both the Langmuir and Sips models were best-fitted. Several adsorbents, particularly carbon adsorbents, present heterogeneous surfaces with different types of binding sites with different binding energies; therefore, they are characterized by a binding affinity distribution function [52]. Thus, although the Langmuir model was a good fit to the data, Langmuir isotherm tends to overcompensate for the curvature in the isotherms, and it is unlikely that the carbon surfaces exhibit homogeneous adsorption of the target molecules on their surfaces. On the other hand, Freundlich isotherm tends to undercompensate the isotherm curvature, assuming an exponential distribution of active centers, which means that the number of available sites is infinite, but this is generally true for the systems where low adsorbate concentrations are involved [52]. The adsorbent/adsorbate systems reached saturation or are close to that.

Table 7. Estimated parameters of the isotherm models adjusted to the experimental data of DCF and PARX adsorption.

	DCF		PARX	
	ACK	CC ^a	ACK	CC ^a
Langmuir				
q_m (mg g ⁻¹)	217	239	276	330
K_L (L mg ⁻¹)	0.2	0.2	0.2	0.03
R^2	0.964	0.841	0.965	0.948
Freundlich				
K_F [mg g ⁻¹ (mg L ⁻¹) ⁿ]	82.5	74.0	102	20.9
n (dimensionless)	5.0	3.9	0.23	1.75
R^2	0.842	0.732	0.953	0.932
Sips				
q_m (mg g ⁻¹)	217	214	275	260
K_S (L mg ⁻¹)	0.099	0.097	0.043	0.024
n_s	0.5	1.66	0.2	1.24
R^2	0.964	0.861	0.965	0.950

^a [29].

Thus, the Sips isotherm model is better to model the linear sub-saturation, as well as the curved saturation portions of the isotherms. Therefore, looking at the results obtained with Sips modeling, the Sips constants for DCF adsorption with both carbons present the same values, indicating a similar affinity of the molecule for the carbon surfaces; however,

the PARX molecule has a higher affinity for ACK carbon when compared to CC carbon. It should be highlighted that the maximum adsorption capacities of both DCF and PARX with ACK carbon are quite high and comparable to the ones obtained with commercial carbon.

The n_s parameter of the Sips model, considered the heterogeneity factor, presents values different from the unity, confirming the presence of heterogeneous surfaces and a Gaussian distribution of the binding sites energy [52,53]. For the systems with CC carbon, the n_s parameter has values above 1, indicating a cooperative reaction between the sorption site and n sorbate molecules [54]. The CC-PARX system presented the highest degree of binding site homogeneity, with an n_s parameter value very close to 1. On the other hand, the n_s parameter has values below 1 for the ACK carbon systems, indicating no cooperation in the binding process.

3.2.4. Temperature Effect

The influence of temperature on the uptake capacities of DCF and PARX by the ACK and CC samples were studied in the range 298–323 K (25–50 °C). The initial concentrations of each adsorbate were 100 mg L⁻¹, and the equilibrium times were the ones chosen in the previous assays. The results present in Figure 9 show that the adsorption of DCF and PARX onto ACK carbon decreases with an increase in the temperature, as well as the adsorption of PARX onto CC carbon. These findings indicate that lower temperatures facilitate adsorption, meaning that an exothermic process is prevalent in those cases. In contrast, the uptake of DCF with CC carbon increases with the temperature, suggesting the prevalence of an endothermic process.

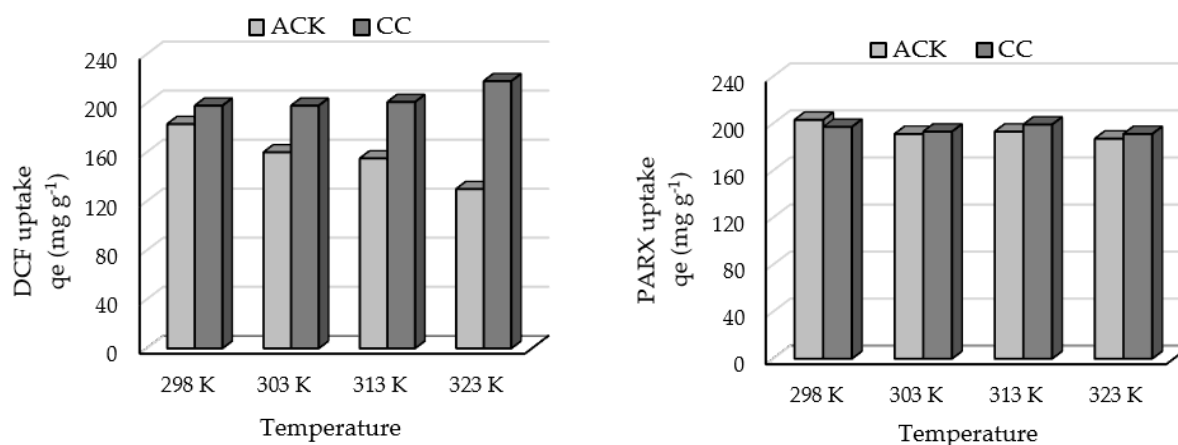


Figure 9. Effect of temperature on the adsorption capacity of DCF and PARX for ACK and CC carbons (Adsorbent mass = 10 mg; Contact time = 8 h (CC carbon) and 4 h (ACK carbon); PARX and DCF initial concentration = 100 mg L⁻¹; Solution volume = 25 mL; Solution initial pH = 6.0 (DCF) and 5.5 (PARX)).

The formation of an adsorption ‘bond’ between sorbate and sorption sites is exothermic by nature [55]. Thus, an endothermic process indicates that the energy released from interactions between CC surface sites and diclofenac molecules is lower than the energy involved in the desolvation of CC surface sites and diclofenac molecules, as well as in the solute–solute interactions on the adsorbent surface [55,56].

3.2.5. Adsorption Mechanisms

It is well-known that organic compounds with aromatic rings can establish π – π dispersive interactions with the graphene layers of carbon materials [57,58]; thus, it must be assumed that this was an important mechanism in the removal of the drugs with both carbons. Since an adsorption process is usually not limited to a single mechanism, it is necessary to go deeper into the adsorbates/adsorbents properties that, together with the results obtained in adsorption assays, allow elucidating the other removal mechanisms

that can be involved. Hydrogen bonding with the electronegative atoms (F, N, and O) of the adsorbate molecules and the electropositive H of the oxygen functional groups [59,60] is highly probable, particularly for ACK carbon, given the fact that this carbon presented a surface richer in the –OH phenolic groups and carboxyl groups (–COOH). Effectively, the Sips constant (Table 7) associated with PARX removal shows that the molecule, with F and N atoms in its structure [43], has a higher affinity for ACK carbon.

Electrostatic attraction should also be considered, particularly in the case of the DCF molecule, which was in its anionic form, while both carbons presented positively charged surfaces. However, CC carbon presents a higher pH_{PZC} (Table 3) and, consequently, has a more positively charged surface, establishing stronger electrostatic interactions with the DCF anionic molecule.

It must be highlighted that the adsorption results correlate poorly with the surface area of adsorbents, since ACK carbon presented a higher surface area and micropore volume (Table 2) than the commercial carbon, but the maximum uptake capacities of DCF and PARX with the two adsorbents were quite comparable. Carbon's pore size and geometry and local energetic environment have a strong influence on the nanoconfinement of the adsorbate molecules [61]. Previous authors have confirmed the critical role of pore size in porous carbons for the adsorption of pharmaceutical molecules [62–64], evidencing how important the tailoring is of the textural properties. Analyzing the micropore size distribution of the carbons (Figure 1), it seems that CC carbon presents more supermicropores (0.7–2 nm), which are usually more favorable for the adsorption of organic molecules [65]; thus, the pore size effect also played a role on the adsorption of DCF and PARX.

Comparing the results obtained in this work with the results previously obtained by the authors, in which argan nutshells were submitted to H_3PO_4 activation [29] and the resulting carbon (ACH) was applied as a removal agent of the same drug molecules, it can be concluded that KOH activation allows obtaining porous carbons with better properties for the removal of this type of adsorbate. Effectively, ACK carbon achieves uptake capacities 46 and 64% higher for DCF and PARX, respectively, compared to ACH carbon. The authors attributed the better performance of ACK carbon to its higher microporosity.

3.2.6. Desorption Studies

The reusability of biomass-derived carbon ACK was then tested up to four cycles of adsorption–desorption by using water as the desorption agent of DCF and PARX. Ultrasonic washing is known to be an effective and easy regeneration method [66], and using water as the washing solvent fulfils the cost and environmental requirements. As shown in Figure 10, the removal efficiency of the pharmaceutical compounds decreased with the consecutive uses of the carbon, this effect more accentuated after the second reuse. This decrease may result from the incomplete removal of DCF and PARX from the carbon surface during the sonication process with water as the solvent; thus, the carbon-active sites become gradually occupied during each cycle [67].

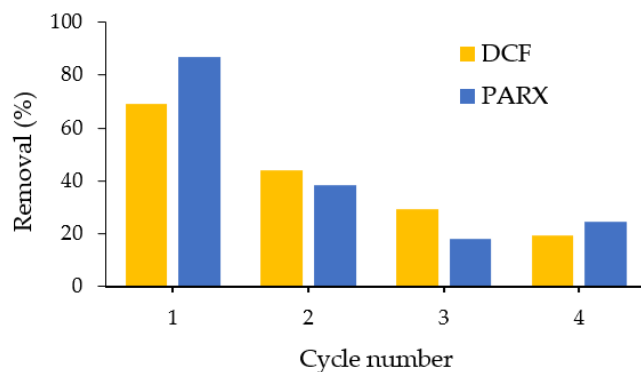


Figure 10. Influence of the regeneration cycle on the removal efficiency of DCF and PARX with ACK carbon.

It was previously demonstrated that organic solvents or even acidic solutions performed better in desorbing pharmaceutical compounds from carbon surfaces [68]. Thus, future assays should be performed with different organic solvents that allow simultaneously a high regeneration efficiency without destroying the porous structure and recovery of the pharmaceutical compounds [69].

Based on these results, no more than one cycle of use of ACK after washing with water should be performed.

4. Conclusions

Argan nutshells were converted into highly porous carbons via two-step activation: in the first step, the biochar was obtained, and in the second step, the biochar was activated with KOH. The experimental design used allowed the conclusion that the sample impregnated at a Biochar/KOH ratio of 1:2 and activated at 800 °C for 1 h presented the higher surface area and developed porosity. Thus, this sample, ACK carbon, was selected for further characterization and applied as an adsorbent of diclofenac (DCF) and paroxetine (PARX) present in synthetic solutions.

Textural (N_2 adsorption isotherms and SEM-EDS) and chemical (pH_{PZC} , FTIR, XPS, and TPD) surface properties of ACK porous carbon were determined and compared to that of a commercial carbon, CC, used as a benchmark. ACK carbon presented a higher surface area and micropore volume ($1624 \text{ m}^2 \text{ g}^{-1}$, $0.40 \text{ cm}^3 \text{ g}^{-1}$) than the CC carbon ($1030 \text{ m}^2 \text{ g}^{-1}$, $0.30 \text{ cm}^3 \text{ g}^{-1}$), but the maximum uptake capacities of DCF ($214\text{--}217 \text{ mg g}^{-1}$) and PARX ($260\text{--}275 \text{ mg g}^{-1}$) obtained from the Sips isotherm model were comparable among the two carbons. Besides the typical $\pi\text{--}\pi$ interactions, H-bonds with the electronegative atoms (F, N, and O) of the adsorbate molecules and the electropositive H of the oxygen functional groups were pointed out as the most probable mechanisms for the adsorption onto ACK porous carbon, given the fact that this carbon presented a surface richer in -OH phenolic groups and carboxyl groups -COOH. The electrostatic attraction was also considered, particularly for the DCF molecule with CC carbon. The pore size might have also been critical, since CC carbon presented more supermicropores (0.7–2 nm), which are usually more favorable for the adsorption of pharmaceutical molecules.

Argan nutshell-derived carbons activated with KOH achieve higher uptake capacities of DCF and PARX than the biomass-based carbons activated with H_3PO_4 , because KOH allows obtaining carbons with higher microporosity.

Based on the results of this study, argan nutshells are valid precursors for developing porous carbons with a high adsorption capacity of DCF and PARX molecules.

Supplementary Materials: The following supporting information can be downloaded at <https://www.mdpi.com/article/10.3390/app12157607/s1>. Figure S1. Molecular structures of the pharmaceutical compounds used in the present study. Figure S2. Calibration curves of DCF and PARX determined by UV-Vis spectrophotometry. Figure S3. N_2 adsorption-desorption isotherms of ACK and CC carbon samples. Figure S4. TGA curves of ANS biomass, biochar, ACK, and CC under argon atmosphere. Figure S5. XPS peak fitted profiles of C 1s and O 1s regions of ACK and CC carbons. Figure S6. TPD spectra of the carbons: (A) CO and (B) CO_2 evolution. Figure S7. SEM image of CC sample with magnification 1500 \times and the corresponding EDS spectrum [29]. Table S1. Equations of the kinetic models and isotherm models used in the present work.

Author Contributions: Conceptualization, A.M., O.B. and M.B.; methodology, A.M., Z.K., M.B., O.S.G.P.S. and A.M.B.D.R.; validation, O.B., A.B., R.F., M.B., I.M., N.L. and M.V.; formal analysis, A.M., Z.K., M.B., O.S.G.P.S. and A.M.B.D.R.; investigation, A.M., M.B., I.M., M.V., O.S.G.P.S. and A.M.B.D.R.; resources, O.B., A.B., R.F., M.B., N.L., O.S.G.P.S., A.M.B.D.R. and I.F.; writing—original draft preparation, A.M. and M.B.; writing—review and editing, A.M., O.B., M.B., I.M., N.L., M.V., O.S.G.P.S., A.M.B.D.R. and I.F.; visualization, A.M. and M.B.; supervision, O.B., M.B. and I.F.; and funding acquisition, O.B., N.L. and I.F. All authors have read and agreed to the published version of the manuscript.

Funding: The first financial support of this work was provided by the Algerian Ministry of Higher Education and by the Directorate General for Scientific Research and Technological Development. This work was also supported by the Associate Laboratory for Green Chemistry—LAQV financed by Portuguese funds from FCT/MCTES (UIDB/50006/2020 and UIDP/50006/2020) and was also financially supported by LA/P/0045/2020 (ALiCE), UIDB/50020/2020, and UIDP/50020/2020 (LSRE-LCM) with Portuguese funds through FCT/MCTES (PIDDAC). OSGP Soares acknowledges FCT funding under the Scientific Employment Stimulus—Institutional Call CEECINST/00049/2018. Maria Bernardo and Márcia Ventura acknowledge the Norma Transitória DL57/2016 Contract (FCT/MCTES).

Institutional Review Board Statement: Not applicable.

Informed Consent Statement: Not applicable.

Data Availability Statement: Not applicable.

Acknowledgments: Asma Mokhati and Oumessaâd Benturki acknowledge the Algerian parliamentarian from Tindouf, Mohamed Messawdja, for having provided the argan seeds.

Conflicts of Interest: The authors declare no conflict of interest.

References

1. Dias, J.M.; Alvim-ferraz, M.C.M.; Almeida, M.F.; Sa, M. Waste materials for activated carbon preparation and its use in aqueous-phase treatment: A review. *J. Environ. Manag.* **2007**, *85*, 833–846. [[CrossRef](#)] [[PubMed](#)]
2. Abuelnoor, N.; Alhajaj, A.; Khaleel, M.; Vega, L.F.; Abu-Zahra, M.R.M. Activated carbons from biomass-based sources for CO₂ capture applications. *Chemosphere* **2021**, *282*, 131111. [[CrossRef](#)] [[PubMed](#)]
3. Da Silva Santos, D.H.; Paulino, J.C.P.L.; dos Santos Alves, G.F.; de Magalhães Oliveira, L.M.T.; de Carvalho Nagliate, P.; da Silva Duarte, J.L.; Meili, L.; Tonholo, J.; Silva Zanta, C.L.P. Effluent treatment using activated carbon adsorbents: A bibliometric analysis of recent literature. *Environ. Sci. Pollut. Res.* **2021**, *28*, 32224–32235. [[CrossRef](#)]
4. González-García, P. Activated carbon from lignocellulosics precursors: A review of the synthesis methods, characterization techniques and applications. *Renew. Sustain. Energy Rev.* **2018**, *82*, 1393–1414. [[CrossRef](#)]
5. Valero-romero, M.J.; Rodríguez-cano, M.Á.; Palomo, J. Carbon-Based Materials as Catalyst Supports for Fischer—Tropsch Synthesis: A Review. *Front. Mater.* **2021**, *7*, 617432. [[CrossRef](#)]
6. Tan, X.F.; Liu, S.-B.; Liu, Y.-G.; Gu, Y.-L.; Zeng, G.-M.; Hu, X.-J.; Wang, X.; Liu, S.-H.; Jiang, L.-H. Biochar as potential sustainable precursors for activated carbon production: Multiple applications in environmental protection and energy storage. *Bioresour. Technol.* **2017**, *227*, 359–372. [[CrossRef](#)] [[PubMed](#)]
7. Thomas, P.; Lai, C.W.; Bin Johan, M.R. Recent developments in biomass-derived carbon as a potential sustainable material for super-capacitor-based energy storage and environmental applications. *J. Anal. Appl. Pyrolysis* **2019**, *140*, 54–85. [[CrossRef](#)]
8. Yahya, M.A.; Al-Qodah, Z.; Ngah, C.W.Z. Agricultural bio-waste materials as potential sustainable precursors used for activated carbon production: A review. *Renew. Sustain. Energy Rev.* **2015**, *46*, 218–235. [[CrossRef](#)]
9. Ben Mansour, R.; Ben Slema, H.; Falleh, H.; Tounsi, M.; Kechebar, M.S.A.; Ksouri, R.; Megdiche-Ksouri, W. Phytochemical characteristics, antioxidant, and health properties of roasted and unroasted Algerian argan (*Argania spinosa*) oil. *J. Food Biochem.* **2018**, *42*, e12562. [[CrossRef](#)]
10. Koufan, M.; Belkoura, I.; Mazri, M.A.; Amarraque, A.; Essatte, A.; Elhorri, H.; Zaddoug, F.; Alaoui, T. Determination of antioxidant activity, total phenolics and fatty acids in essential oils and other extracts from callus culture, seeds and leaves of *Argania spinosa* (L.) Skeels. *Plant Cell Tissue Organ Cult.* **2020**, *141*, 217–227. [[CrossRef](#)]
11. Goik, U.; Goik, T.; Załęska, I. The Properties and Application of Argan Oil in Cosmetology. *Eur. J. Lipid Sci. Technol.* **2019**, *121*, 1800313. [[CrossRef](#)]
12. Karoune, S.; Belhamra, M.; Kechebar, M.S.A.; Rahmoune, C. Characterization of the argan tree of southwestern Algeria. *Int. J. Curr. Microbiol. Appl. Sci.* **2013**, *2*, 117–126.
13. El Khomri, M.; El Messaoudi, N.; Dbik, A.; Bentahar, S.; Lacherai, A. Efficient adsorbent derived from *Argania Spinosa* for the adsorption of cationic dye: Kinetics, mechanism, isotherm and thermodynamic study. *Surf. Interfaces* **2020**, *20*, 100601. [[CrossRef](#)]
14. Akhzouz, H.; El Minor, H.; Tatane, M.; Bendarma, A. Physical characterization of bio-composite CEB stabilized with Argan nut shell and cement. *Mater. Today Proc.* **2021**, *36*, 107–114. [[CrossRef](#)]
15. Essabir, H.; Achaby, M.E.I.; Hilali, E.M.; Bouhfid, R.; Qaiss, A.E. Morphological, Structural, Thermal and Tensile Properties of High Density Polyethylene Composites Reinforced with Treated Argan Nut Shell Particles. *J. Bionic Eng.* **2015**, *12*, 129–141. [[CrossRef](#)]
16. Elmouwahidi, A.; Zapata-benabithe, Z.; Carrasco-marín, F.; Moreno-castilla, C. Activated carbons from KOH-activation of argan (*Argania spinosa*) seed shells as supercapacitor electrodes. *Bioresour. Technol.* **2012**, *111*, 185–190. [[CrossRef](#)] [[PubMed](#)]
17. Zbair, M.; Ainassaari, K.; El Assal, Z.; Ojala, S.; El Ouahedy, N.; Keiski, R.L.; Bensitel, M.; Brahmi, R. Steam activation of waste biomass: Highly microporous carbon, optimization of bisphenol A, and diuron adsorption by response surface methodology. *Environ. Sci. Pollut. Res.* **2018**, *25*, 35657–35671. [[CrossRef](#)] [[PubMed](#)]

18. Boujibar, O.; Ghosh, A.; Achak, O.; Chafik, T.; Ghamouss, F. A high energy storage supercapacitor based on nanoporous activated carbon electrode made from Argan shells with excellent ion transport in aqueous and non-aqueous electrolytes. *J. Energy Storage* **2019**, *26*, 100958. [[CrossRef](#)]
19. Dahbi, M.; Kiso, M.; Kubota, K.; Horiba, T.; Hida, K.; Matsuyama, T.; Komaba, S. Synthesis of hard carbon from argan shells for Na-ion batteries. *J. Mater. Chem. A* **2017**, *5*, 9917–9928. [[CrossRef](#)]
20. Boujibar, O.; Souikny, A.; Ghamouss, F.; Achak, O.; Dahbi, M.; Chafik, T. CO₂ capture using N-containing nanoporous activated carbon obtained from argan fruit shells. *J. Environ. Chem. Eng.* **2018**, *6*, 1995–2002. [[CrossRef](#)]
21. Zbair, M.; Ainassaari, K.; Drif, A.; Ojala, S.; Bottlinger, M.; Pirilä, M.; Keiski, R.L.; Bensitel, M.; Brahmi, R. Toward new benchmark adsorbents: Preparation and characterization of activated carbon from argan nut shell for bisphenol A removal. *Environ. Sci. Pollut. Res.* **2018**, *25*, 1869–1882. [[CrossRef](#)] [[PubMed](#)]
22. Zbair, M.; Bottlinger, M.; Ainassaari, K.; Ojala, S.; Stein, O.; Keiski, R.L.; Bensitel, M.; Brahmi, R. Hydrothermal Carbonization of Argan Nut Shell: Functional Mesoporous Carbon with Excellent Performance in the Adsorption of Bisphenol A and Diuron. *Waste Biomass Valorization* **2020**, *11*, 1565–1584. [[CrossRef](#)]
23. Mohan, H.; Rajput, S.S.; Jadhav, E.B.; Sankhla, M.S.; Sonone, S.S.; Jadhav, S.; Kumar, R. Ecotoxicity, occurrence, and removal of pharmaceuticals and illicit drugs from aquatic systems. *Biointerface Res. Appl. Chem.* **2021**, *11*, 12530–12546. [[CrossRef](#)]
24. Reyes, N.J.D.G.; Geronimo, F.K.F.; Yano, K.A.V.; Guerra, H.B.; Kim, L. Pharmaceutical and Personal Care Products in Different Matrices: Occurrence, Pathways, and Treatment Processes. *Water* **2021**, *13*, 1159. [[CrossRef](#)]
25. Khasawneh, O.F.S.; Palaniandy, P. Occurrence and removal of pharmaceuticals in wastewater treatment plants. *Process Saf. Environ. Prot.* **2021**, *150*, 532–556. [[CrossRef](#)]
26. Shahid, M.K.; Kashif, A.; Fuwad, A.; Choi, Y. Current advances in treatment technologies for removal of emerging contaminants from water—A critical review. *Coord. Chem. Rev.* **2021**, *442*, 213993. [[CrossRef](#)]
27. Shamsudin, M.S.; Azha, S.F.; Ismail, S. A review of diclofenac occurrences, toxicology, and potential adsorption of clay-based materials with surfactant modifier. *J. Environ. Chem. Eng.* **2022**, *10*, 107541. [[CrossRef](#)]
28. Silva, L.J.G.; Pereira, A.M.P.T.; Meisel, L.M.; Lino, C.M.; Pena, A. Reviewing the serotonin reuptake inhibitors (SSRIs) footprint in the aquatic biota: Uptake, bioaccumulation and ecotoxicology. *Environ. Pollut.* **2015**, *197*, 127–143. [[CrossRef](#)]
29. Mokhati, A.; Benturki, O.; Bernardo, M.; Kecira, Z.; Matos, I.; Lapa, N.; Ventura, M.; Soares, O.S.G.P.; do Rego, A.M.B.; Fonseca, I.M. Nanoporous carbons prepared from argan nutshells as potential removal agents of diclofenac and paroxetine. *J. Mol. Liq.* **2021**, *326*, 115368. [[CrossRef](#)]
30. Ferreira, A.C.; Ferraria, A.M.; do Rego, A.M.B.; Gonçalves, A.P.; Correia, M.R.; Gasche, T.A.; Branco, J.B. Partial oxidation of methane over bimetallic nickel-lanthanide oxides. *J. Alloys Compd.* **2010**, *498*, 316–323. [[CrossRef](#)]
31. Tomczyk, A.; Sokołowska, Z.; Boguta, P. Biochar physicochemical properties: Pyrolysis temperature and feedstock kind effects. *Rev. Environ. Sci. Bio/Technol.* **2020**, *19*, 191–215. [[CrossRef](#)]
32. Chowdhury, Z.Z.; Hamid, S.B.A.; Das, R.; Hasan, M.R.; Zain, S.M.; Khalid, K.; Uddin, M.N. Preparation of carbonaceous adsorbents from lignocellulosic biomass and their use in removal of contaminants from aqueous solution. *BioResources* **2013**, *8*, 6523–6555. [[CrossRef](#)]
33. Ahmed, M.B.; Hasan Johir, M.A.; Zhou, J.L.; Ngo, H.H.; Nghiem, L.D.; Richardson, C.; Moni, M.A.; Bryant, M.R. Activated carbon preparation from biomass feedstock: Clean production and carbon dioxide adsorption. *J. Clean. Prod.* **2019**, *225*, 405–413. [[CrossRef](#)]
34. Yu, B.; Chang, Z.; Wang, C. The key pre-pyrolysis in lignin-based activated carbon preparation for high performance supercapacitors. *Mater. Chem. Phys.* **2016**, *181*, 187–193. [[CrossRef](#)]
35. Mayoral, E.P.; Matos, I.; Bernardo, M.; Durán-Valle, C.; Fonseca, I. Functional porous carbons: Synthetic strategies and catalytic application in fine chemical synthesis. In *Emerging Carbon Materials for Catalysis*; Elsevier: Amsterdam, The Netherlands, 2021; pp. 299–352.
36. Heidarinejad, Z.; Dehghani, M.H.; Heidari, M.; Javedan, G.; Ali, I.; Sillanpää, M. Methods for preparation and activation of activated carbon: A review. *Environ. Chem. Lett.* **2020**, *18*, 393–415. [[CrossRef](#)]
37. Thommes, M.; Kaneko, K.; Neimark, A.V.; Olivier, J.P.; Rodriguez-Reinoso, F.; Rouquerol, J.; Sing, K.S.W. Physisorption of gases, with special reference to the evaluation of surface area and pore size distribution (IUPAC Technical Report). *Pure Appl. Chem.* **2015**, *87*, 1051–1069. [[CrossRef](#)]
38. Coates, J. Interpretation of Infrared Spectra, A Practical Approach. In *Encyclopedia of Analytical Chemistry*; John Wiley & Sons, Ltd.: Chichester, UK, 2006.
39. Beamson, G.; Briggs, D. *High Resolution XPS of Organic Polymers, the Scienta ESCA300 Database*; Chichester, Ed.; Wiley: New York, NY, USA, 1992; Volume 5.
40. Figueiredo, J.L.; Pereira, M.F.R.; Freitas, M.M.A.; Órfão, J.J.M. Modification of the surface chemistry of activated carbons. *Carbon* **1999**, *37*, 1379–1389. [[CrossRef](#)]
41. Marya, E.; Alfatah, T.; Dani, M. Synthesis and characterization of activated carbon from *Bambusa vulgaris striata* using two-step KOH activation. *Integr. Med. Res.* **2020**, *9*, 6278–6286. [[CrossRef](#)]
42. Yoo, S.H.; Kang, J.K.; Lee, S.C.; Jang, H.Y.; Kim, S.B. Analysis of adsorption characteristics of diclofenac to sucrose-derived carbon spheres from aqueous solutions. *J. Environ. Chem. Eng.* **2021**, *9*, 106573. [[CrossRef](#)]

43. Carvalho, P.S.; Diniz, L.F.; Tenorio, J.C.; Souza, M.S.; Franco, C.H.J.; Rial, R.C.; Warszawski De Oliveira, K.R.; Nazario, C.E.D.; Ellena, J. Pharmaceutical paroxetine-based organic salts of carboxylic acids with optimized properties: The identification and characterization of potential novel API solid forms. *CrystEngComm* **2019**, *21*, 3668–3678. [[CrossRef](#)]
44. Lagergren, S. About the theory of so-called adsorption of soluble substances. *Sven. Vetenskapsakad. Handlingar*. **1898**, *24*, 1–39.
45. Ho, Y. Review of second-order models for adsorption systems. *J. Hazard. Mater.* **2006**, *136*, 681–689. [[CrossRef](#)] [[PubMed](#)]
46. Hubbe, M.A.; Azizian, S.; Douven, S. Implications of apparent pseudo-second-order adsorption kinetics onto cellulosic materials: A review. *BioResources* **2019**, *14*, 7582–7626. [[CrossRef](#)]
47. Tan, K.L.; Hameed, B.H. Insight into the adsorption kinetics models for the removal of contaminants from aqueous solutions. *J. Taiwan Inst. Chem. Eng.* **2017**, *74*, 25–48. [[CrossRef](#)]
48. Langmuir, I. The constitution and fundamental properties of solids and liquids. II. Liquids. *J. Am. Chem. Soc.* **1917**, *39*, 1848–1906. [[CrossRef](#)]
49. Freundlich, H. Über die Adsorption in Lösungen. *Zeitschrift für Phys. Chemie* **1907**, *57U*, 385–470. [[CrossRef](#)]
50. Sips, R. On the structure of a catalyst surface. *J. Chem. Phys.* **1948**, *16*, 490–495. [[CrossRef](#)]
51. Al-Ghouti, M.A.; Da'ana, D.A. Guidelines for the use and interpretation of adsorption isotherm models: A review. *J. Hazard. Mater.* **2020**, *393*, 122383. [[CrossRef](#)]
52. Kumar, K.V.; Gadipelli, S.; Wood, B.; Ramisetty, K.A.; Stewart, A.A.; Howard, C.A.; Brett, D.J.L.; Rodriguez-Reinoso, F. Characterization of the adsorption site energies and heterogeneous surfaces of porous materials. *J. Mater. Chem. A* **2019**, *7*, 10104–10137. [[CrossRef](#)]
53. Kumar, K.V.; Serrano-Ruiz, J.C.; Souza, H.K.S.; Silvestre-Albero, A.M.; Gupta, V.K. Site energy distribution function for the sips isotherm by the condensation approximation method and its application to characterization of porous materials. *J. Chem. Eng. Data* **2011**, *56*, 2218–2224. [[CrossRef](#)]
54. Wan, X.; Lee, J.W.; Row, K.H. Nonlinear isotherm of benzene and its derivatives by frontal analysis. *Korean J. Chem. Eng.* **2009**, *26*, 182–188. [[CrossRef](#)]
55. Shahwan, T. Critical insights into the limitations and interpretations of the determination of ΔG_0 , ΔH_0 , and ΔS_0 of sorption of aqueous pollutants on different sorbents. *Colloids Interface Sci. Commun.* **2021**, *41*, 100369. [[CrossRef](#)]
56. Leone, V.O.; Pereira, M.C.; Aquino, S.F.; Oliveira, L.C.A.; Correa, S.; Ramalho, T.C.; Gurgel, L.V.A.; Silva, A.C. Adsorption of diclofenac on a magnetic adsorbent based on maghemite: Experimental and theoretical studies. *New J. Chem.* **2018**, *42*, 437–449. [[CrossRef](#)]
57. Radovic, L.R.; Silva, I.F.; Ume, J.I.; Menéndez, J.A.; Leon, Y.; Leon, C.A.; Scaroni, A.W. An experimental and theoretical study of the adsorption of aromatics possessing electron-withdrawing and electron-donating functional groups by chemically modified activated carbons. *Carbon* **1997**, *35*, 1339–1348. [[CrossRef](#)]
58. Moreno-Castilla, C. Adsorption of organic molecules from aqueous solutions on carbon materials. *Carbon* **2004**, *42*, 83–94. [[CrossRef](#)]
59. Kah, M.; Sigmund, G.; Xiao, F.; Hofmann, T. Sorption of ionizable and ionic organic compounds to biochar, activated carbon and other carbonaceous materials. *Water Res.* **2017**, *124*, 673–692. [[CrossRef](#)] [[PubMed](#)]
60. Barquilha, C.E.R.; Braga, M.C.B. Adsorption of organic and inorganic pollutants onto biochars: Challenges, operating conditions, and mechanisms. *Bioresour. Technol. Rep.* **2021**, *15*, 100728. [[CrossRef](#)]
61. Cárdenas, H.; Müller, E.A. How does the shape and surface energy of pores affect the adsorption of nanoconfined fluids? *AIChE J.* **2021**, *67*, e17011. [[CrossRef](#)]
62. Moral-Rodríguez, A.I.; Leyva-Ramos, R.; Ania, C.O.; Ocampo-Pérez, R.; Isaacs-Páez, E.D.; Carrales-Alvarado, D.H.; Parra, J.B. Tailoring the textural properties of an activated carbon for enhancing its adsorption capacity towards diclofenac from aqueous solution. *Environ. Sci. Pollut. Res.* **2019**, *26*, 6141–6152. [[CrossRef](#)]
63. Mestre, A.S.; Pires, J.; Nogueira, J.M.F.; Carvalho, A.P. Activated carbons for the adsorption of ibuprofen. *Carbon* **2007**, *45*, 1979–1988. [[CrossRef](#)]
64. Fu, H.; Yang, L.; Wan, Y.; Xu, Z.; Zhu, D. Adsorption of Pharmaceuticals to Microporous Activated Carbon Treated with Potassium Hydroxide, Carbon Dioxide, and Steam. *J. Environ. Qual.* **2011**, *40*, 1886–1894. [[CrossRef](#)] [[PubMed](#)]
65. Viegas, R.M.C.; Mestre, A.S.; Mesquita, E.; Campinas, M.; Andrade, M.A.; Carvalho, A.P.; Rosa, M.J. Assessing the applicability of a new carob waste-derived powdered activated carbon to control pharmaceutical compounds in wastewater treatment. *Sci. Total Environ.* **2020**, *743*, 140791. [[CrossRef](#)] [[PubMed](#)]
66. Omorogie, M.O.; Babalola, J.O.; Unuabonah, E.I. Regeneration strategies for spent solid matrices used in adsorption of organic pollutants from surface water: A critical review. *Desalination Water Treat.* **2016**, *57*, 518–544. [[CrossRef](#)]
67. Salvador, F.; Martin-Sanchez, N.; Sanchez-Hernandez, R.; Sanchez-Montero, M.J.; Izquierdo, C. Regeneration of carbonaceous adsorbents. Part II: Chemical, Microbiological and Vacuum Regeneration. *Microporous Mesoporous Mater.* **2015**, *202*, 277–296. [[CrossRef](#)]
68. Mansour, F.; Al-Hindi, M.; Yahfoufi, R.; Ayoub, G.M.; Ahmad, M.N. The use of activated carbon for the removal of pharmaceuticals from aqueous solutions: A review. *Rev. Environ. Sci. Biotechnol.* **2018**, *17*, 109–145. [[CrossRef](#)]
69. Zanella, O.; Tessaro, I.C.; Féris, L.A. Desorption- and decomposition-based techniques for the regeneration of activated carbon. *Chem. Eng. Technol.* **2014**, *37*, 1447–1459. [[CrossRef](#)]